Chemical Communications

Water-soluble non-aggregating zinc phthalocyanine and in vitro study for photodynamic therapy

Electronic Supplementary Information

Saad Makhseed,*[a] Miloslav Machacek,[b] Waleed Alfadly,[a] Ahmad Tuhl,[a] Mickey Vinodh,[a] Tomas Simunek,[b] Veronika Novakova,[c] Pavel Kubat,[d] Emil Rudolf,[e] and Petr Zimcik*[f]

[a] *Department of Chemistry, Kuwait University, P.O. Box 5969, Safat, 13060, Kuwait. Fax: +965 24816482; Tel: +965 24985538; E-mail: saad.makhseed@ku.edu.kw*
[b] *Department of Biochemical Sciences, Faculty of Pharmacy in Hradec Kralove, Charles University in Prague, Heyrovskeho 1203, 500 05, Hradec Kralove, Czech Republic*
[c] *Department of Biophysics and Physical Chemistry, Faculty of Pharmacy in Hradec Kralove, Charles University in Prague, Heyrovskeho 1203, 500 05, Hradec Kralove, Czech Republic*
[d] *J. Heyrovsky Institute of Physical Chemistry, v.v.i., Academy of Sciences of the Czech Republic, Dolejskova 3, 182 23 Praha 8, Czech Republic.*
[e] *Department of Medical Biology and Genetics, Faculty of Medicine in Hradec Kralove, Charles University in Prague, Šimkova 870, Hradec Kralove, Czech Republic*
[f] *Department of Pharmaceutical Chemistry and Drug Control, Faculty of Pharmacy in Hradec Kralove, Charles University in Prague, Heyrovskeho 1203, 500 05, Hradec Kralove, Czech Republic. Fax: +420 495067167; Tel: +420 495067257 E-mail: petr.zimcik@faf.cuni.cz*

Content

Synthesis

Ethanol (EtOH), methanol (MeOH), dichloromethane (DCM), ethyl acetate, tetrahydrofuran (THF), chloroform ($CHCl_3$), *N*,*N*-dimethylformamide (DMF), dimethylsulphoxide (DMSO), dioxane, *n*-hexane, 1-pentanol, quinoline (freshly distilled twice over calcium hydride), and acetone were used as either supplied or dried as described by Perrin and Armarego before use.[1] 1*H*-Imidazol, 2,6-bis(hydroxymethyl)-4-methylphenol, deuterated chloroform ($CDCl_3$), deuterated dimethylsulphoxide (DMSO-d_6), potassium carbonate (K_2CO_3), hydrochloric acid (32% HCl), anhydrous magnesium sulphate ($MgSO_4$), anhydrous sodium sulphate (Na_2SO_4), 1,8-diazabicyclo[5.4.0]undec-7-ene (DBU), anhydrous zinc acetate, and unsubstituted zinc phthalocyanine (ZnPc) were purchased from Sigma-Aldrich. 5,6-Dichlorophthalonitrile was obtained from TCI (Toshima, Japan). Column chromatography was performed using Merck silica gel 60 of mesh size 0.040-0.063 mm. Thin layer chromatography (TLC) was performed using Polygram sil G/UV 254 TLC plates and visualization was by an ultraviolet light at 254 nm and 350 nm. ^{1}H NMR spectra were recorded by using a Bruker DPX 400 MHz super-conducting NMR spectrometer. IR spectra were recorded on a Perkin Elmer system 2000 FTIR. Elemental analyses were carried out using Elemental Vario Micro Cube. Mass analyses were done by electron impact (EI) and fast atom bombardment (FAB) on a Thermo DFS mass spectrometer. DSC analyses were carried out on Shimadzu DSC-50. UV-vis spectra were recorded on Varian Cary 5 spectrometer or Shimadzu UV-2401PC spectrophotometer.

*Synthesis of 2,6-bis((1H-imidazol-1-yl)methyl))-4-methylphenol (**1**):*

Synthesis of compound **1** was adopted from literature with slight modifications.[2] A solution of 1*H*-imidazol (1.7 g, 6.34 mmol) and 2,6-bis(hydroxymethyl)-4-methylphenol (2 g, 10.10 mmol) in dry dioxane (30 mL) was refluxed for 24 h. Thereafter, the solvent was evaporated by removing the condenser to yield a gummy solid which was recrystallized from *n*-hexane to give a white powder (2 g, 54%), mp 190.6 °C, Found: C, 67.58; H, 6.40; N, 20.26%. $C_{15}H_{16}N_4O$ requires C, 67.15; H, 6.01; N, 20.88%; ν_{max} (KBr)/cm^{-1} 3122, 3101, 2966, 1508, δ_H (400 MHz; DMSO-d_6; Me_4Si, 25 °C), 2.11 (3H, s, Me), 5.14 (4H, s, CH_2), 6.77 (2H, s), 6.87 (2H, s), 7.12 (2H, s), 7.67 (2H, s, Ar-H), 9.13 (OH, s); *m/z* (EI) = 268 (M^+, 63%). The data corresponded well with those published.[2]

*Synthesis of 4,5-bis(2,6-bis((1H-imidazol-1-yl)methyl)-4-methylphenoxy)phthalonitrile (**2**):*

Finely ground anhydrous potassium carbonate (10 g, 72 mmol) was added to a stirred solution of **1** (6.6 g, 24.6 mmol) and 4,5-dichlorophthalonitrile (2.3 g, 11.6 mmol) in dry DMF (10 mL). The reaction mixture was heated at 90 °C under nitrogen for 24 h. Upon cooling, the reaction mixture was poured into distilled water (500 ml). The resulting precipitate was collected by filtration and washed with water and air-dried. The crude product was recrystallized from *n*-hexane, to give a yellow powder (4 g, 45%); mp. 258.6 °C, Found: C, 68.23; H, 4.98; N, 20.50%. $C_{38}H_{32}N_{10}O_2$ requires C, 69.08; H, 4.88, N, 21.20%; ν_{max} /cm^{-1} 3112, 2968, 2232 (CN), 1501; δ_H (400 MHz, DMSO-d_6, Me_4Si), 2.28 (6H, s, Me), 5.13 (8H, s, CH_2), 6.86 (4H, s, Ar-H), 6.94 (4H, s, =N-C***H***=CH), 6.99 (2H, s, Pc-Ar-H), 7.12 (4H, s, =N-CH=C***H***), 7.62 (4H, s, N-CH-N). *m/z* (EI) = 660 (M^+, 5%).

*Synthesis of quaternised phthalonitrile (**3**):*

A solution iodomethane (1.8 g, 12.2 mmol) and **2** (2 g, 3.03 mmol) in dry DMF (20 mL) was heated at 80 °C under nitrogen atmosphere for 24 h. The reaction mixture was poured into acetone (100 mL) to give a brownish precipitate which was collected by filtration and washed with hot ethyl acetate. The crude product was refluxed in acetone and filtered three times to give a yellow solid (2 g, 54%); mp 350.6 °C, Found: C, 39.86; H, 3.78, N, 10.99%. $C_{42}H_{44}N_{10}O_2I_4$ requires C, 41.06; H, 3.61; N, 11.40%; ν_{max}/cm^{-1} 3061, 2971, 2229 (CN), 1564, 1477; δ_H (400 MHz, DMSO-d$_6$, Me$_4$Si), 2.37 (6H, s, Me), 3.87 (12H, s, NMe), 5.34 (8H, s, CH_2), 7.22 (4H, s, Ar-H), 7.32 (2H, s, Pc-Ar-H), 7.63 (4H, s, =N-C***H***=CH), 7.73 (4H, s, =N-CH=C***H***), 9.10 (4H, s, N-CH-N); δ_H (400 MHz, D_2O, Me$_4$Si, 25 °C), 2.24 (6H, s, Me), 3.78 (12H, s, NMe), 5.27 (8H, s, CH_2), 7.11 (4H, s, Ar-H), 7.17 (2H, s, Pc-Ar-H), 7.35 (12H, s); *m/z* (FAB) = 1228.1 (M^+, 3%), 1101.9 ([M-I$^-$]$^+$, 100%).

*Synthesis of 2,3,9,10,16,17,23,24-octa(2,6-bis((1H-imidazol-1-yl)methyl)-4-methylphenoxy)phthalocyanine zinc(II) (**4**):*

A mixture of **2** (1 g, 1.51 mmol) and anhydrous zinc(II) acetate (0.092 g, 0.50 mmol) in dry 1-pentanol (5 mL) was refluxed under nitrogen for 8 h. The reaction mixture was cooled to room temperature and poured into distilled water (100 mL). The green precipitate was collected by filtration and washed with hot water and ethyl acetate subsequently. The crude product was recrystallized from ethyl acetate to yield a green solid ($C_{152}H_{128}N_{40}O_8Zn$, 0.3 g, 29%), mp > 300 °C; *m/z* = 2705 (M^+, 10%). The ^{1}H NMR spectrum of the complex in DMSO-d$_6$ showed complex splitting patterns with broad and overlapped signals. Addition of few drops of pyridine-d$_5$ did not improve the quality of the spectrum.

*Synthesis of quaternised phthalocyanine (**5**):*

A solution of **4** (0.8 g, 0.295 mmol) and iodomethane (3 g, 21.1 mmol) in dry DMF (20 mL) was heated at 80 °C for 24 h under nitrogen. The collected crude product was purified by recrystallization from acetone to give complex **5** as a green solid (0.3 g, 20%), mp > 300 °C, Found: C, 39.61; H, 3.47; N, 11.16%. $C_{168}H_{176}I_{16}N_{40}O_8Zn$ + 6 H_2O requires C, 39.66; H, 3.72; N, 11.01%; λ_{max}(DMF)/nm 681 (ε/dm^3 mol^{-1} cm^{-3} 239 900), λ_{max}(H_2O)/nm 682 (ε/dm^3 mol^{-1} cm^{-3} 208 900); ν_{max}/cm^{-1} 3077, 1613, 1569, 1478, 1449; δ_H (400 MHz, DMSO-d$_6$, Me$_4$Si), 2.66 (24H, s, Me), 3.69 (48H, s, NMe), 5.73 (32H, s, CH_2), 7.62 (16H, s, Ar-H), 7.70 (16H, s, =N-C***H***=CH), 7.79 (16H, s, =N-CH=C***H***), 8.06 (8H, s, Pc-Ar-H), 9.21 (16H, s, N-CH-N); δ_H (400 MHz, D_2O, Me$_4$Si), 2.50 (24H, s, Me), 3.37 (48H, s, NMe), 5.51 (32H, s, CH_2), 7.13 (16H, s, Ar-H), 7.41 (16H, s, =N-C***H***=CH), 7.44 (16H, s, =N-CH=C***H***), 8.55 (8H, s, Pc-Ar-H), 8.74 (16H, s, N-CH-N).

^{1}H NMR spectra

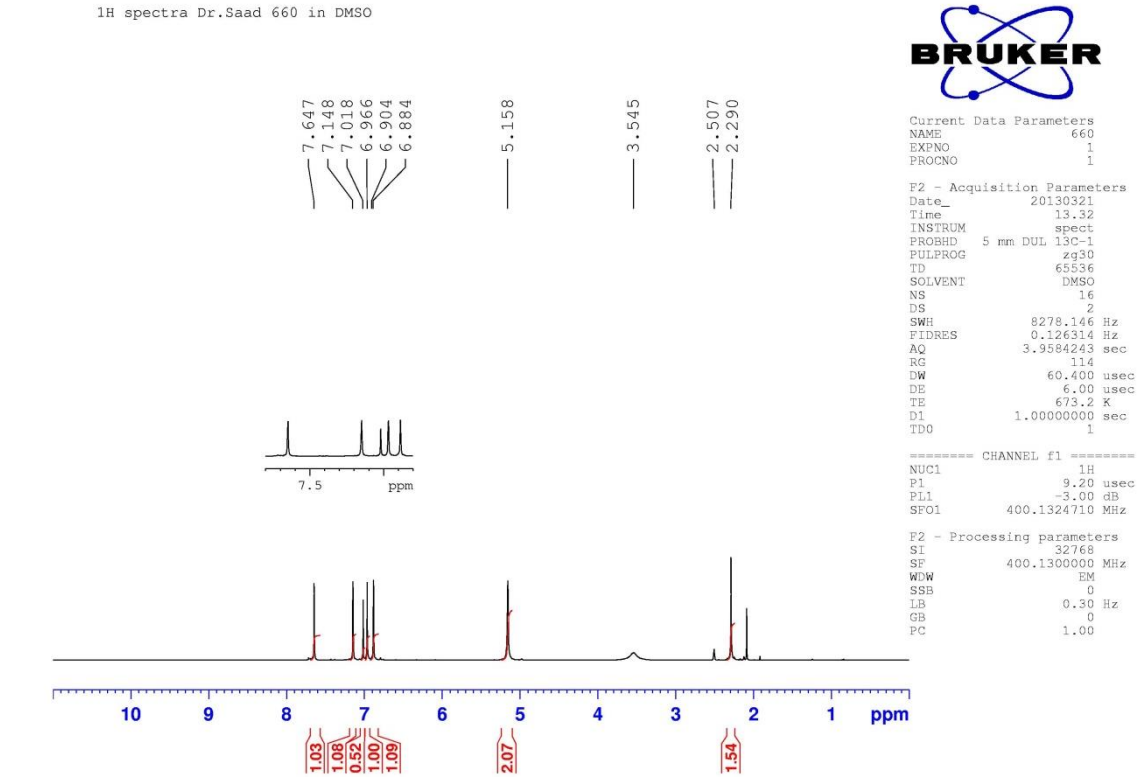

Fig S1. ^{1}H NMR spectrum of compound **2** in DMSO-d_6.

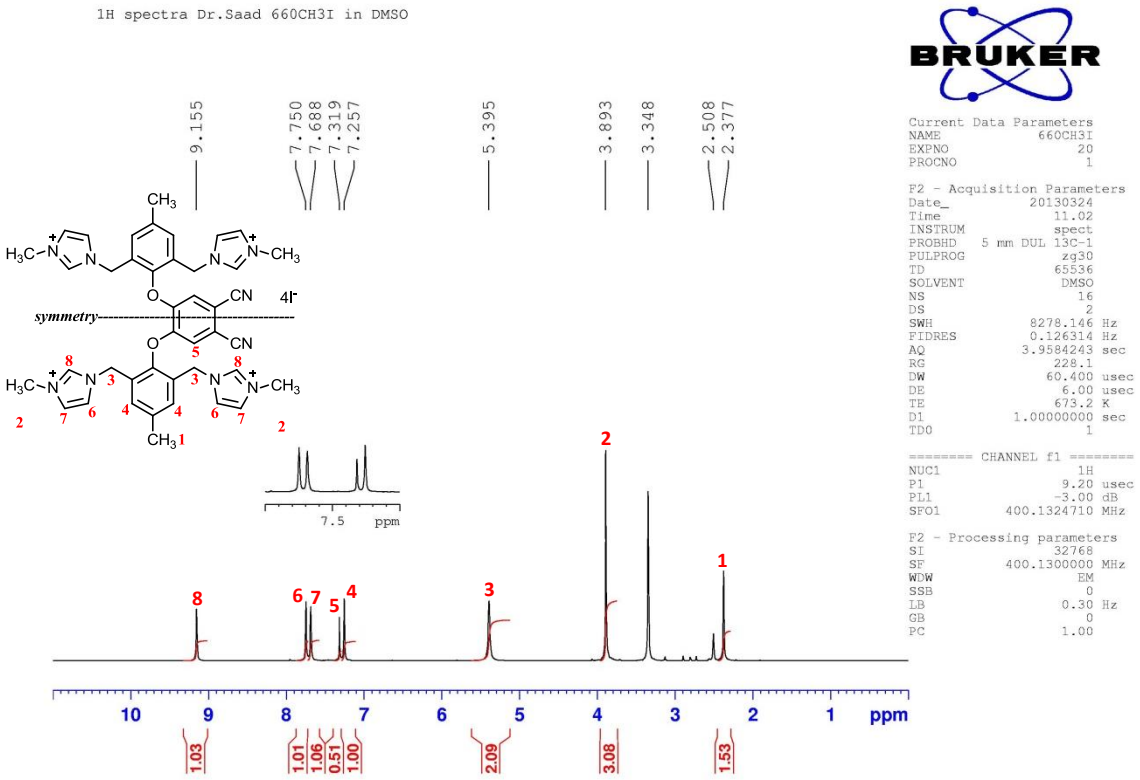

Fig. S2. ^{1}H NMR spectrum of compound **3** in DMSO-d_6.

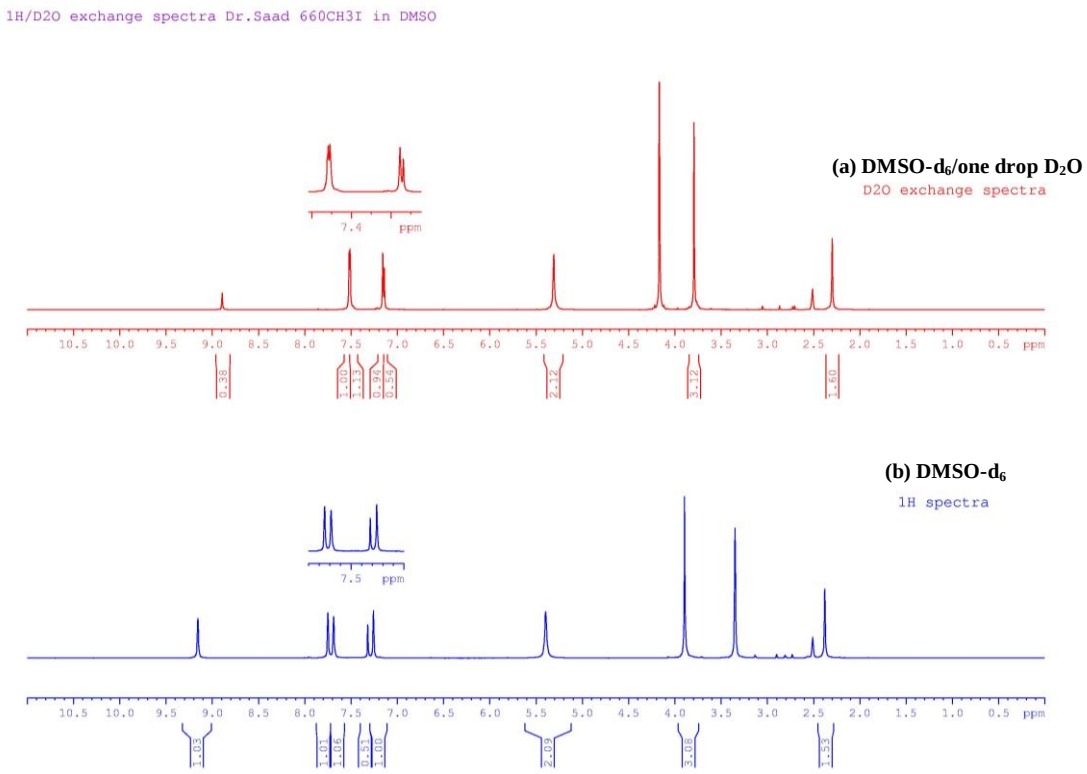

Fig. S3. ^{1}H NMR spectra of compound **3** recorded in **(a)** DMSO-d_6 and one drop of D_2O; **(b)** DMSO-d_6 showing the acidity of proton numbered 8 according to the structure depicted in Fig. S2 by exchanging with D_2O.

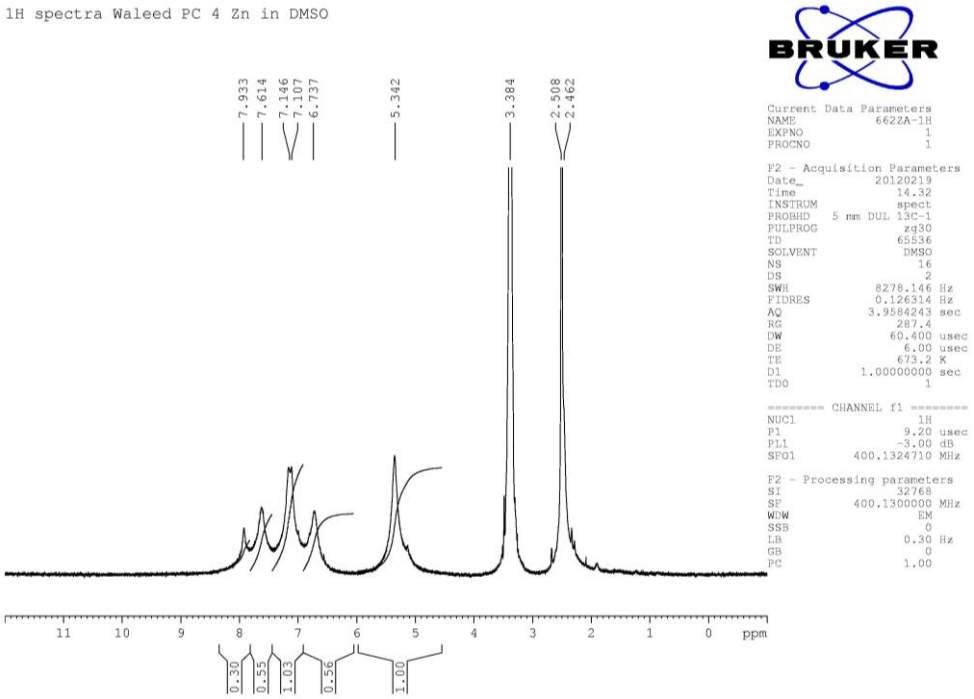

Fig. S4. ^{1}H NMR spectra of compound **4** recorded in DMSO-d_6.

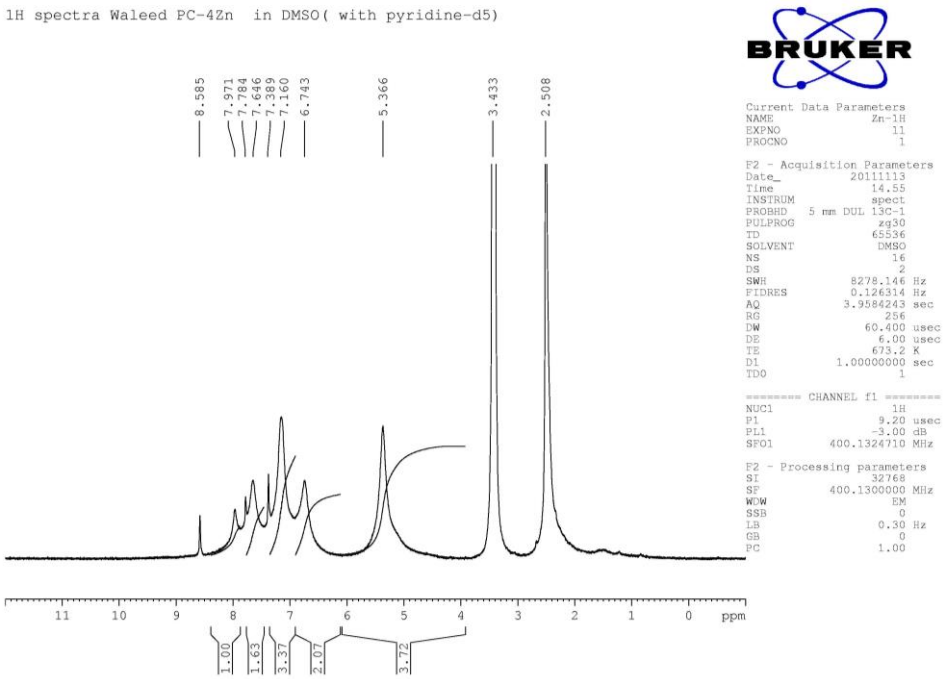

Fig. S5. ^{1}H NMR spectra of compound **4** recorded in DMSO-d_6 after addition of pyridine-d_5.

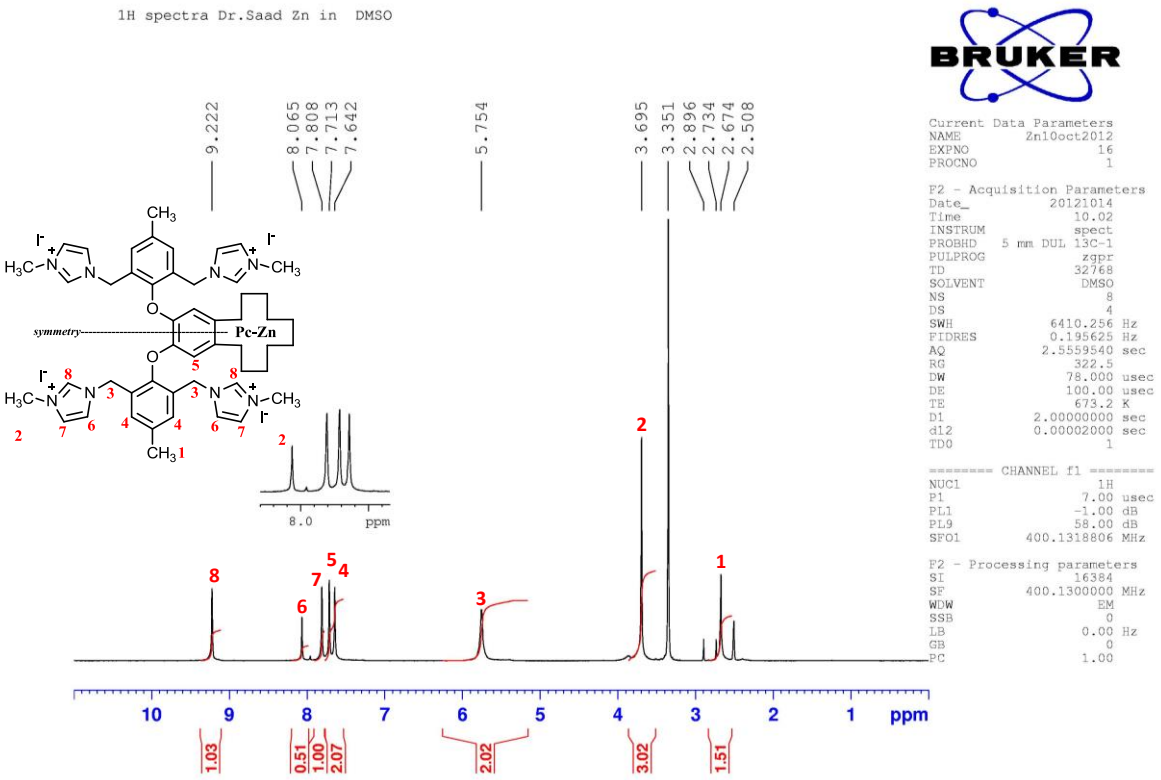

Fig. S6. ^{1}H NMR spectrum of complex **5** in DMSO-d_6.

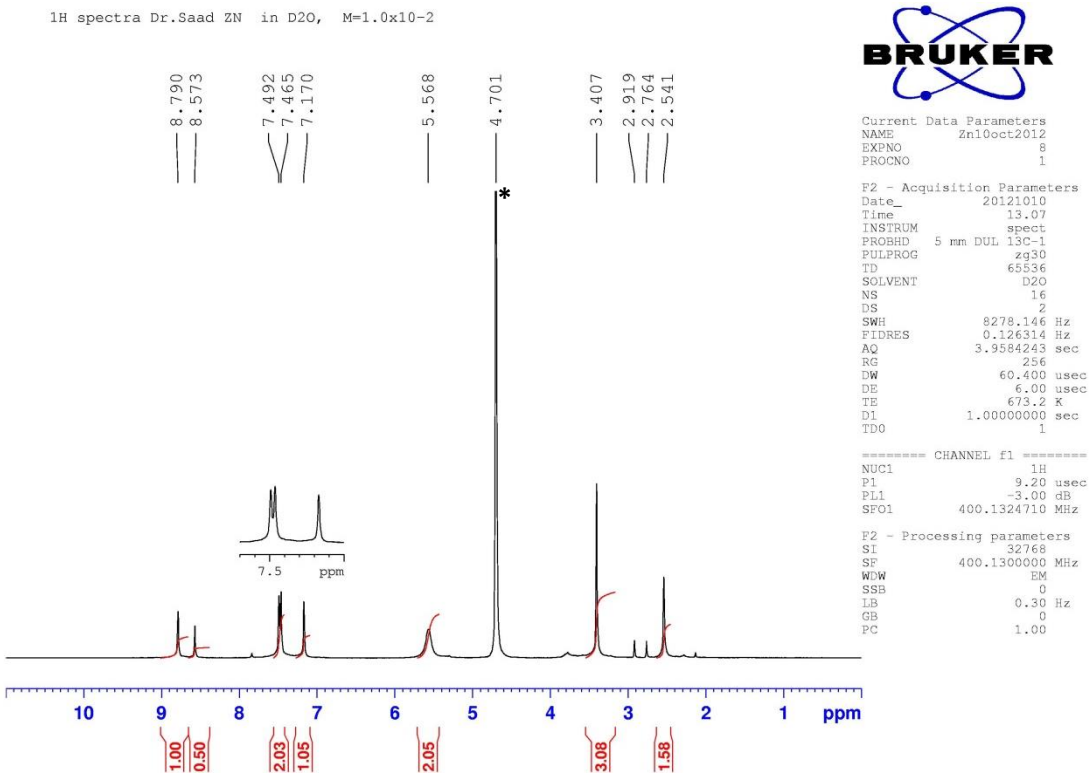

Fig. S7. ^{1}H NMR spectrum of complex **5** in D_2O at concentration 10.0 mM.

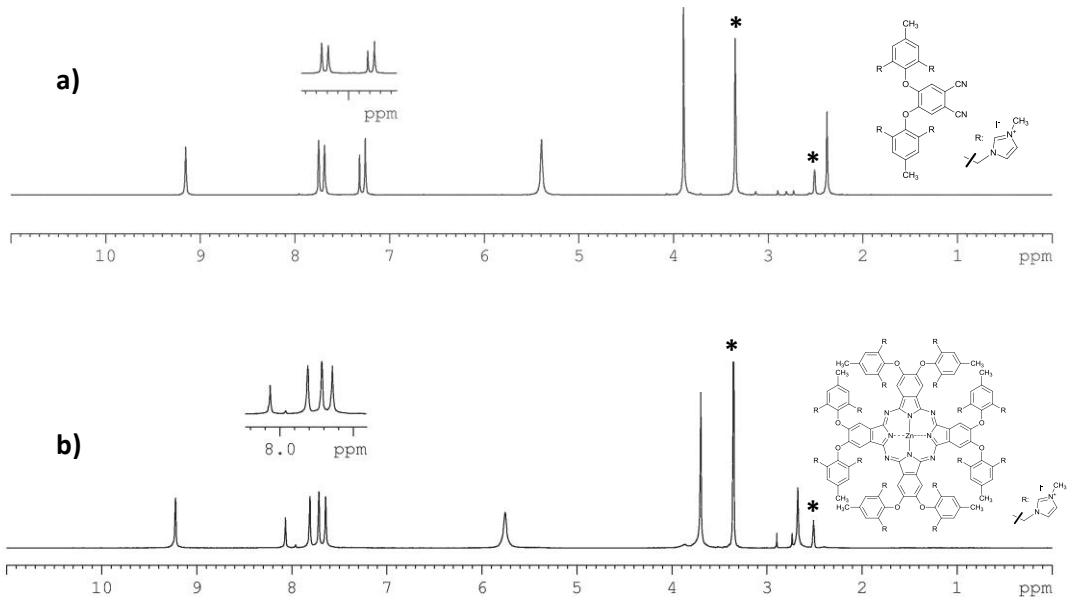

Fig. S8. Comparison of ^{1}H NMR spectra of compound **3** (a) and complex **5** (b) measured in DMSO-d_6. Asterisks (*) indicate residuals of non-deuterated solvent and water.

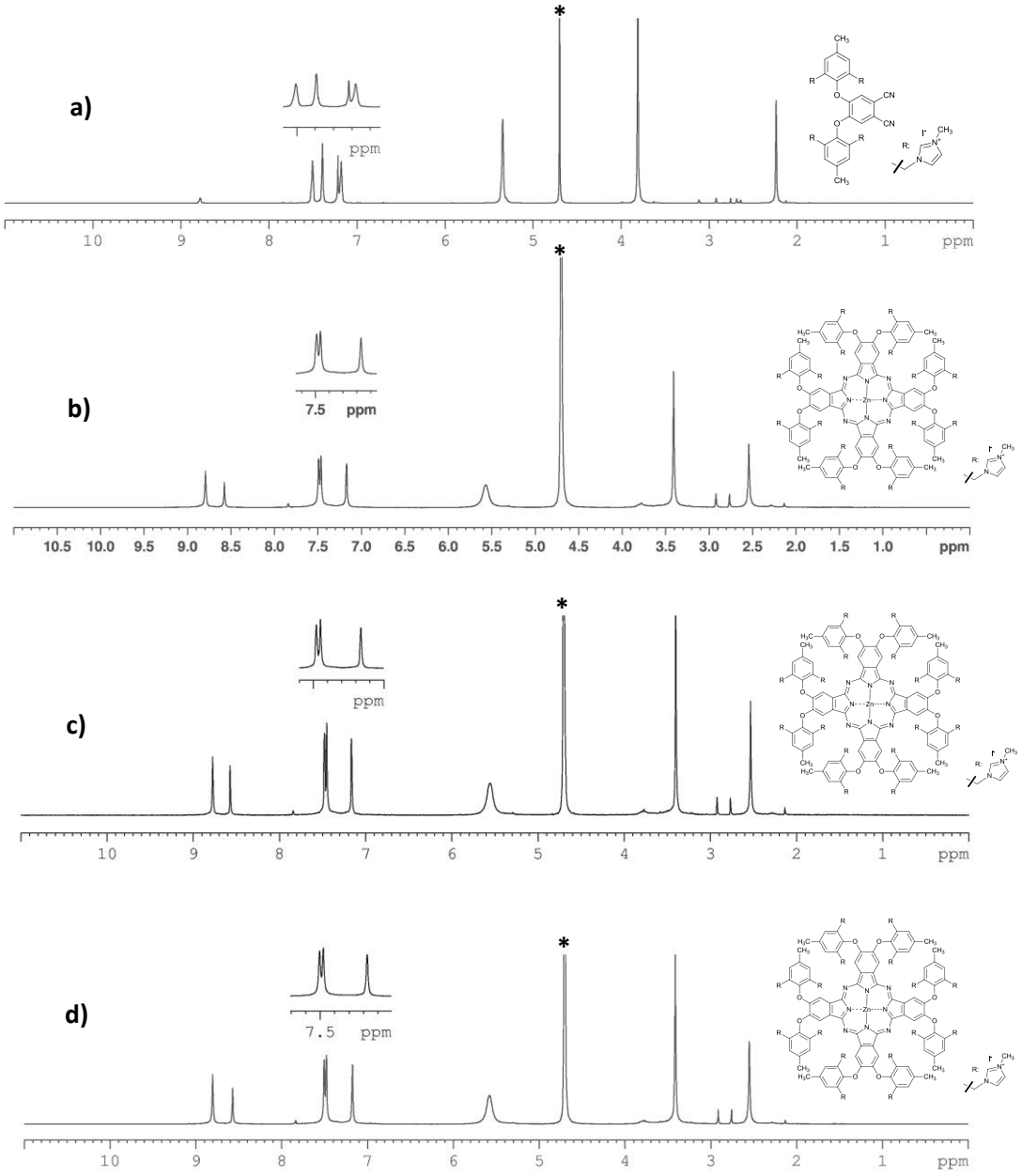

Fig. S9. ^{1}H NMR spectra of compound **3** (a) and complex **5** (b-d) measured in D_2O. Concentration of complex **5** was 6.67 mM (b), 2.9 mM (c) and 20 mM (d). Asterisk (*) indicates residual of non-deuterated water.

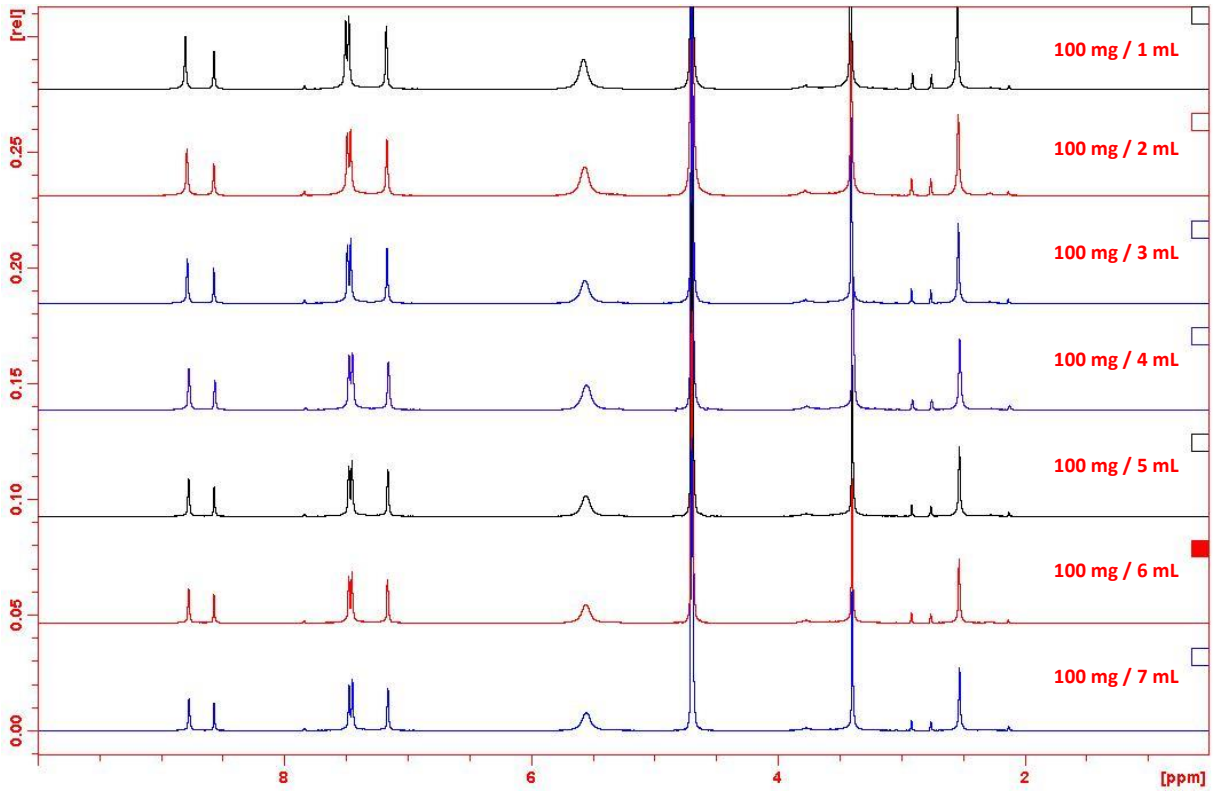

Fig. S10. ^{1}H NMR spectra of complex **5** at different concentrations in D_2O.

Discussions on crystal data of phthalonitrile precursor 2 and its quaternized derivative 3.

Single crystals suitable for X-ray diffraction technique were grown by solvent diffusion method. Out of various solvent combinations tried for crystal growth, hexane-THF system was most successful for **2** whereas water-THF was suitable in the case of **3**.

All single crystal data collections were made on a Rigaku R-AXIS RAPID diffractometer using filtered Mo-Kα radiation. The data were collected at a temperature of -123 °C (Oxford cryosystems). The structure was solved by direct methods[3] and expanded using Fourier techniques. The non-hydrogen atoms were refined anisotropically. Hydrogen atoms were refined using the riding model. All calculations were performed using the crystallographic software (Crystal Structure 4.0: Crystal Structure Analysis Package, Rigaku Corporation (2000-2010). Tokyo 196-8666, Japan) package except for refinement, which was performed using SHELXL-97.[3] Table S1 sums up crystal description and various single crystal diffraction parameters of **2** and **3.**

Table S1. Summary on the nature of the crystals and various diffraction parameters of **2** and **3.**

Compound	**2**	**3**
Crystal dimension / mm	0.300 × 0.250 × 0.200	0.200 × 0.100 × 0.050
Crystal Shape	Block	Platelet
Formula weight	$C_{38}H_{32}N_{10}O_2$	$C_{42}H_{44}I_4N_{10}O_2$
Crystal system	Triclinic	Monoclinic
Space group (no.)	P-1 (2)	$P2_1/n$(14)
T/ °C	-123 ±1	-123
a/Å	10.415(4)	13.3100(7)
b//Å	13.601(4)	15.3725(7)
c/Å	15.135(5)	23.689(2)
α/deg	100.335(7)	90.000
β/deg	108.711(9)	90.067(7)
γ/deg	106.981(8)	90.000
V/ $Å^3$	1852(1)	4846.9(5)
Z	2	4
μ (MOKα)	0.775 cm^{-1}	26.164 cm^{-1}
ρ_{calcd}/g cm^{-3}	1.185	1.683
$2\theta_{max}$/deg	50.1	54.9
Reflections collected	14293	43208
Unique reflections	6508	11086
R_{int}	0.0484	0.0325
R (I > 2σ)	0.1423	0.0411
R (all data)	0.1806	0.0495
R_w(all data)	0.4437	0.1009
$\lvert\Delta\rho\rvert_{max}$ e $Å^{-3}$	0.43	1.36

The molecular structure information obtained from single crystal X- diffraction method is in perfect agreement with the predicted synthetic protocol and other characterization techniques like NMR and mass spectroscopy.

The ORTEP representation of structures **2** and **3** are depicted in Figure S11. As expected the aromatic plane of the phenoxy functions containing imidazole moieties lies almost perpendicular to the plane of phthalonitrile moiety owing to steric constrains. In the case of **2,** the calculated torsion angles of the chain of atoms C1-O1-C7-C8 is -96.0, C1-O1-C7-C12 is 90.2, C6-O2-C24-C25 is 91.4 and C6-O2-C24-C29 is -96.0 which confirms that the dihedral angles between the phenyl ring containing phthalonitrile functional groups are more or less 90 degrees to the plane of those phenoxy functions. The four imidazoyl functions were mutually directed as widely as possible to minimize steric constraints. The 3-dimensional packing structure of this molecule, viewing along a-, b- and c- directions are given in Figure S12, which provides a clear idea of the networking pattern of this system in the crystal. Along a- direction the molecules are arranged in parallel lines and all are in the same orientation. The b- direction also showed all molecules arranged in same orientation and

line. On the other hand, along c- direction two neighboring molecules in the same line are oppositely directed to each other. Thus orientation of nitrile groups along c- is same for 1,3,5,... molecules while in 2,4,6… molecules those are directed in opposite direction. This type of arrangement enabled **2** to minimize the void volumes in its crystal structure and allowed its imidazole nitrogens to stay in the range of intermolecular H-bonding positions with suitable hydrogen atoms.

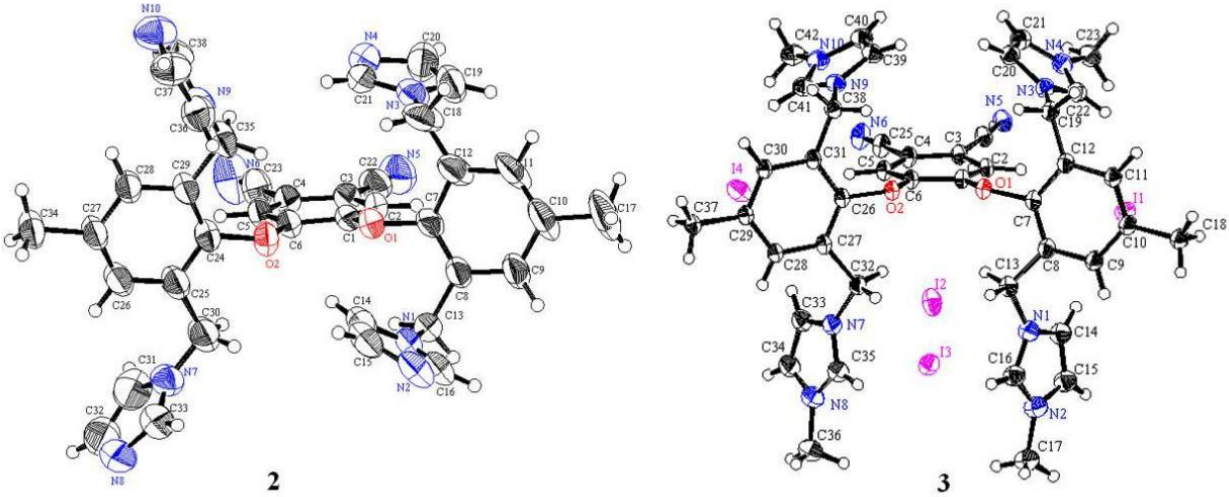

Fig.S11. ORTEP representation (50% probability) of the crystal structures of phthalonitrile precursor **2** and quaternized derivative **3**. Color code: red - oxygen; blue - nitrogen; gray –carbon; purple - iodine; white –hydrogen.

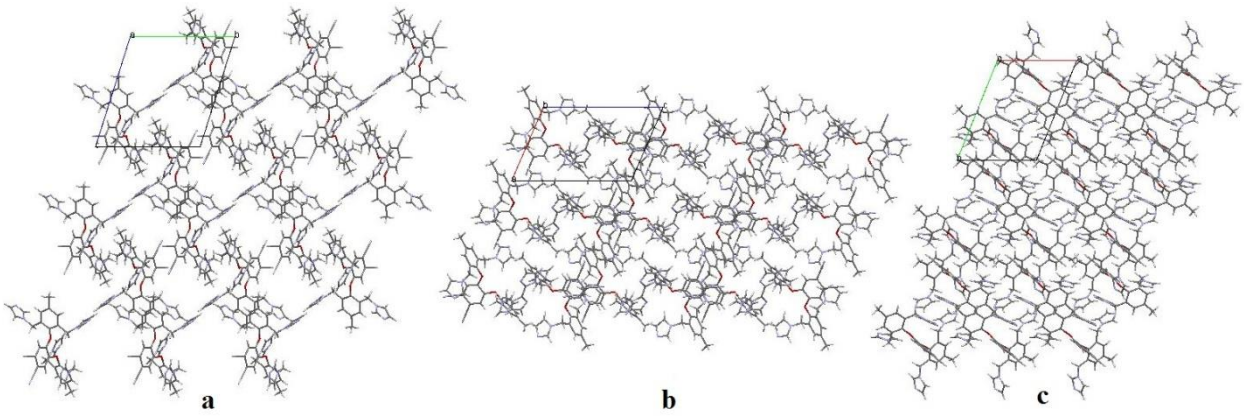

Fig. S12. 3-dimensional packing diagram of **2** viewing along a-, b- and c- directions. Color code: red - oxygen; blue - nitrogen; dark gray –carbon; purple - iodine; light gray – hydrogen.

The orientation of different imidazoyl moieties in the structure of quaternized phthalonitrile precursor **3** and the overall packing of these molecules in the crystal network is different from that of its nonmethylated counterpart **2**. The ORTEP structure of this quaternized molecule is also given in Figure S11. In this case too, the orthogonal orientation between the aromatic planes of the phenoxy substituents and the plane of phthalonitrile core is confirmed from the crystal structure and the dihedral angles are only marginally varied from that of the **2** (the torsion angle C1-O1-C7-C8 is -92.4, C1-O1-C7-C12 is 97.7, C6-O2-C26-

C27 is 90.3 and C6-O2-C26-C31 is -97.4). At the same time, the orientations of the methyl imidazole groups are remarkably varied from that of the relative imidazole positions of **2** (Figure S13 and Table S2). This change in orientations can easily be explained from the steric point of view when considering the situation to adapt bulky iodide counter anions.

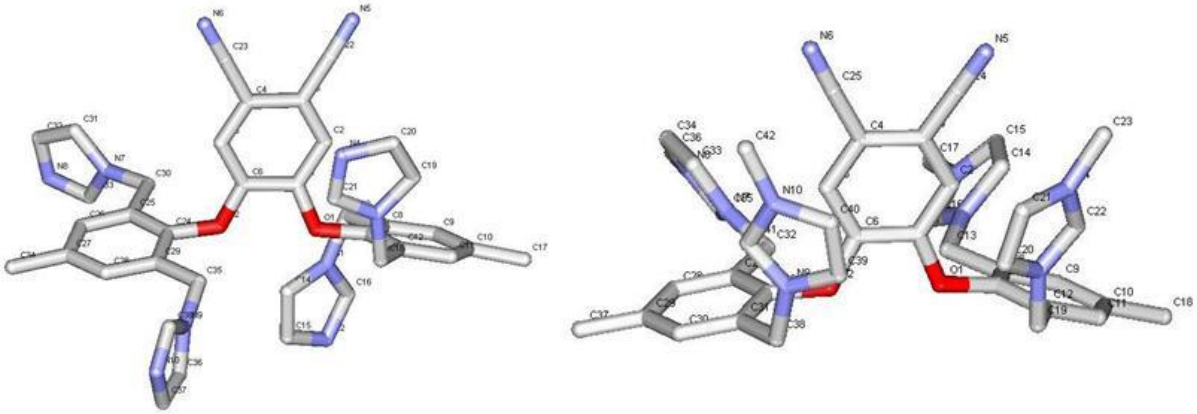

Fig. S13. relative positions of imidazolyl groups in **2** and **3**. Color code: red - oxygen; blue - nitrogen; gray –carbon; iodine and hydrogen atoms are omitted for clarity.

Table S2. Torsion angles of imidazolyl functions with basic structural unit of **2** and **3**.

2		**3**	
Atom sequence	Torsion angle	Atom sequence	Torsion angle
C7-C12-C18-N3	-84.9	C7-C12-C19-N3	-77.5
C11-C12-C18-N3	99.5	C11-C12-C19-N3	105.2
C9-C8-C13-N1	91.4	C9-C8-C13-N1	-27.2
C7-C8-C13-N1	-85.1	C7-C8-C13-N1	154.8
C24-C29-C35-N9	-157.8	C26-C31-C38-N9	80.0
C28-C29-C35-N9	24.8	C30-C31-C38-N9	-100.2
C24-C25-C30-N7	176.9	C26-C27-C32-N7	-155.0
C26-C25-C30-N7	0.4	C28-C27-C32-N7	27.3

The 3-dimensional packing diagram of **3** units is also different from that **2**. Unlike the crystal network observed in **2**, the molecules of **3** form a zig-zag arrangement with wider channels in the crystal structure along the a- direction. This is clearly observed when viewing the packing pattern through the c- direction (Figure S14c). These channels are found to be occupied by iodide anions (Figure S14). The space filling illustration of the 3-dimensional packing with and without iodine ions clearly demonstrates the occupancy of iodine ions in the vacant sites in the structure. The space filling structure without iodine ions when viewing through all three directions clearly shows these channels as vacant voids. So it can be confirmed that the orientations of methyl imidazoyl functions are rearranged considerably so as to provide more vacant space in the network to accommodate the bulky iodide units.

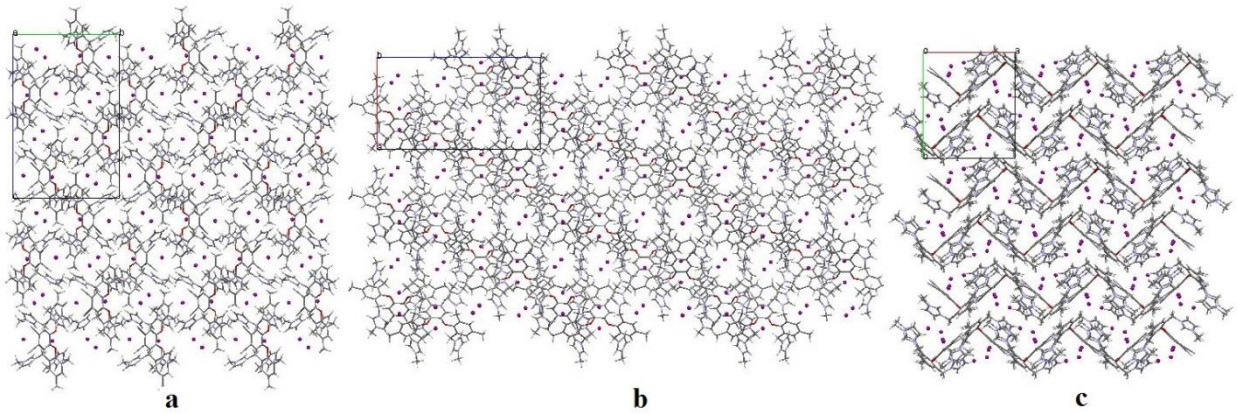

Fig. S14. 3-dimensional packing diagram of **3** viewing along a-, b- and c- directions. Color code: red - oxygen; blue - nitrogen; dark gray –carbon; purple - iodine; light gray – hydrogen.

Absorption spectra in water-based media.

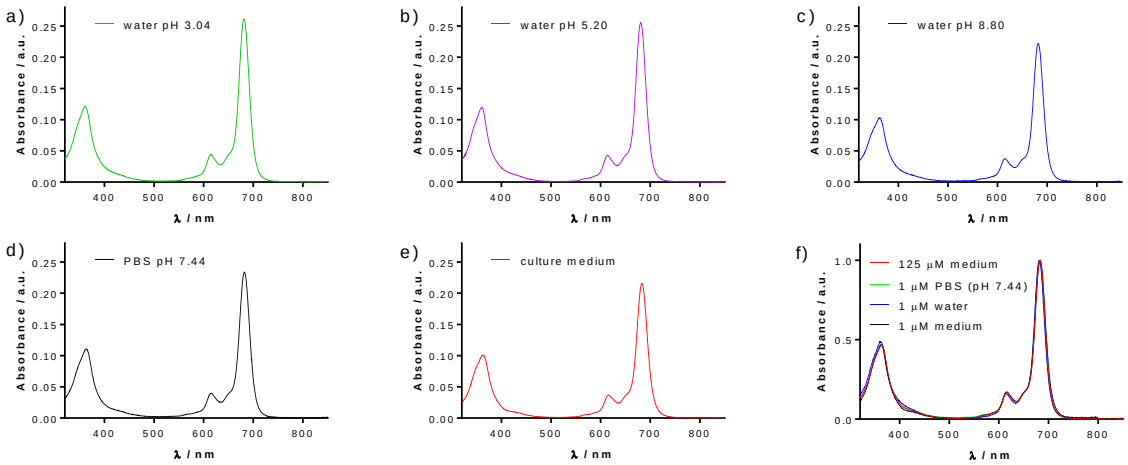

Fig. S15. Absorption spectra of compound **5** at concentration of 1 µM in a) water pH 3.04 (achieved by addition of HCl), b) water pH 5.20 (distilled water), c) water pH 8.80 (achieved by addition of NaOH), d) phosphate buffered saline pH 7.44 (PBS, Sigma), e) culture medium (DMEM including FBS, for composition see section Cell cultures). f) Selected spectra (normalized to the same absorption at Q-band) combined into one graph. Graph f) indicates no influence of any additives (pH, buffer salts, proteins in medium, etc.) on the aggregation of compound **5** as deduced form the perfectly overlapping spectra.

Partition coefficient

n-Octanol (2 mL) was added to a solution of compound **5** (2 mL, approx. 50 μM) in PBS (pH 7.44). The mixture was vortexed for 5 min and then centrifuged (16 800 g, rt, 10 min) to separate the phases. The absorption spectra of both organic and water phase (Figure S16) were measured after diluting a sample 50-fold into DMF. No absorption in Q-band area was detected in organic phase leading to conclusion that partition coefficient (*P*) of **5** is reaching a zero value.

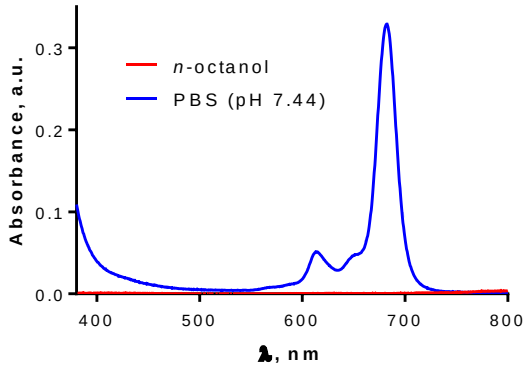

Fig. S16. Absorption spectra of **5** in DMF in partition coefficient experiment. The sample was prepared by diluting *n*-octanol (red) and water (blue) phases into DMF.

Photophysical measurements

Fluorescence measurements.

Fluorescence quantum yields (Φ_F) of complex **5** were determined in water and DMF by the comparative method using ZnPc as a reference (Φ_F = 0.32 in THF[4]). Both reference and sample were excited at 611 nm. Φ_F was calculated using Equation S1:

$$\Phi_F^S = \Phi_F^R \left(\frac{F^S}{F^R}\right)\left(\frac{1-10^{-A^R}}{1-10^{-A^S}}\right)\left(\frac{n^S}{n^R}\right)^2 \qquad \text{(Eq. S1)}$$

where F is the integrated area under the emission spectrum, A is absorbance at excitation wavelength, n is the refractive index of the solvent. Superscripts R and S correspond to the reference and sample, respectively. All experiments were performed three times and data represent a mean of these three experiments. Estimated error ± 15%. Excitation spectra were collected by observing the fluorescence signal at λ_{em} = 745 nm. Absorption in Q-band was always below 0.05 in order to reduce inner filter effect.

Fluorescence lifetime measurements were measured using an Fluoromax 4 (Horiba Jobin Yvon) spectroflurometer. Lifetime measurements were carried out employing laser-diode excitation at 611 nm (NanoLED-605, Pulse duration: 1.5 ns, peak wavelength 611 nm). The emission was recorded at fluorescence maxima using a cooled Fluorohub photon detection module in a time-correlated single photon counting (TCSPC) setup. The decay curves were fitted to exponential functions through the iterative reconvolution procedure of the DAS6 software (v6.6, Horiba Jobin Yvon).

Transient absorption measurements.

The samples were excited with a Lambda Physik COMPEX 102 excimer (308 nm, pulse width 28 ns) or a Lambda Physik FL 3002 dye (670 nm, ca. 1 mJ/ pulse) lasers. The corresponding transient absorption spectra (Figure S17) were measured within 350-800 nm on a laser kinetic spectrometer LKS 20 (Applied Photophysics, U.K.). The time profiles (Figure S18, Table S3) of the triplet states at a maximum of T-T absorption band (500 nm) were recorded using a 150 W Xe lamp (Phillips) equipped with a pulse unit and a R928 photomultiplier (Hamamatsu). Where appropriate, the samples were saturated by oxygen or argon.

The rate constants k_q for the quenching of the triplet states by oxygen were calculated using linear Stern-Volmer equation:

$$1/\tau_T = 1/\tau_T^{Ar} + k_q\,[O_2], \quad \text{(Eq. S2)}$$

where τ_T is lifetime of the triplet states (in oxygen-, air- or Ar- saturated solution). The corresponding concentrations of molecular oxygen [O_2] were estimated from litererature data (3.14 mM in oxygen-saturated DMF[5] and 0.27 mM in air-saturated water[6]) and Henry´s law constants.

Table S3. Summary of triplet state lifetimes (τ_T, in μs) of compound **5** in different solvents saturated by selected gases.

Solvent	Argon saturated	Air saturated	Oxygen saturated
DMF	170	2.1	0.55
D_2O	73	6.0	1.6

Luminescence of singlet oxygen.

The time-resolved near-infrared luminescence of $O_2(^1\Delta_g)$ at 1270 nm was monitored using a Ge detector (Judson J16-8SP-R05M-HS) upon laser excitation at 308 or 670 nm. The signal from the detector was collected on a 600 MHz Agilent Infiniium oscilloscope and transferred to a computer for further analysis. The signal-to-noise ratio of the signals was improved by the averaging of 200 individual traces. The short-lived signal produced by the scattering of an excitation laser pulse and phthalocyanine fluorescence was eliminated by exciting the argon-saturated sample and subtracting the obtained signal from the signal recorded in air-saturated solutions (Figure S19). The temporal profile of the luminescence was fitted to a single-

exponential decay function with the exclusion of the initial portion of the plot, which was affected by the formation of singlet oxygen from the phthalocyanine triplets. The initial luminescences were extrapolated from the curve-fitting and they were proportional to the excitation energy. The quantum yields of singlet oxygen formation in air-saturated solution, Φ_Δ, were estimated by the comparative method using unsubstituted ZnPc (excitation at 670 nm, Φ_Δ =0.56 in DMF[7]), tetrakis(4-sulfonatophenyl)porphyrin (TPPS, excitation at 308 nm, Φ_Δ = 0.62 in D_2O[8]) and methylene blue (MB, excitation at 308 nm, Φ_Δ = 0.52 in D_2O[8]) as references.

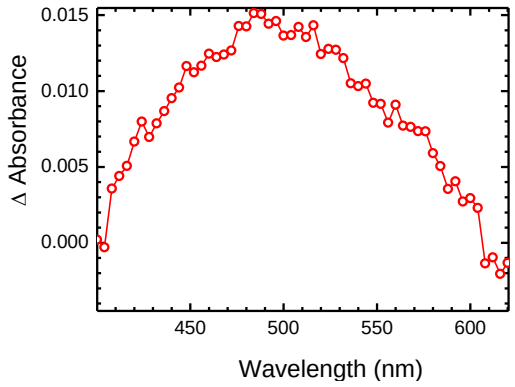

Fig. S17. Transient absorption spectra (compound **5**) 500 ns after excitation by a 670 nm laser pulse in air-saturated D_2O, average of 10 traces.

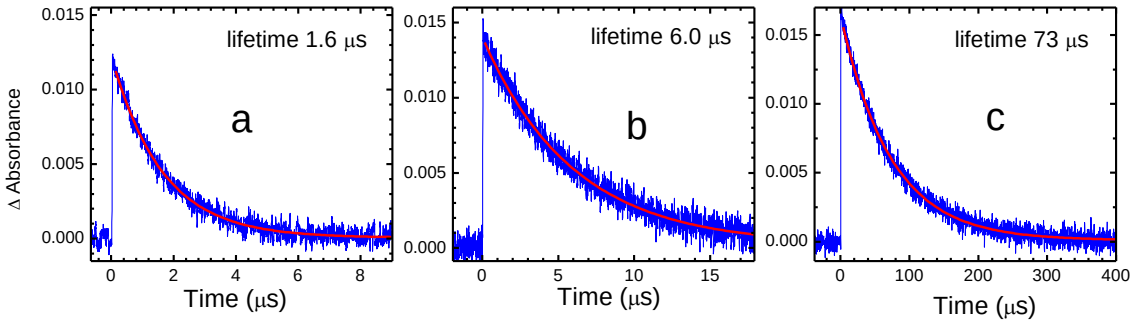

Fig. S18. Decay of the triplet states of **5** in oxygen- (a), air- (b), and argon-(c) saturated D_2O, average of 10 traces. The red lines are least-squares monoexponential fits. Monitored at 500 nm.

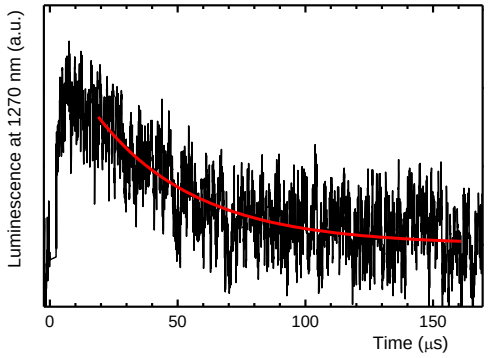

Fig. S19. Luminescence of $O_2(^1\Delta_g)$ calculated as difference between luminescence in air- and argon-saturated D_2O after excitation of **5** by a 670 nm laser pulse at a low excitation energy (380 μJ), average of 200 traces. The red line is a least-squares monoexponential fit.

In vitro cytotoxicity assessments

Cell cultures

The 3T3 and HeLa cell lines were obtained from the American Type Cell Culture Collection (ATCC, U.S.A.). Cells were cultured in Dulbecco's modified Eagle's medium (DMEM) without Phenol Red (Lonza, Belgium) supplemented with 10 % heat-inactivated fetal bovine serum (FBS, Lonza), 1 % penicillin/streptomycin solution (Lonza), 10 mM HEPES buffer (Sigma, Germany) and 4 mM L-glutamine (Lonza). Each cell line was cultured in 75 cm^2 tissue culture flasks (TPP, Switzerland) at 37 °C in a humidified atmosphere of 5% CO_2. Sub-confluent cells were subcultured every 3-4 days. For dark toxicity and photodynamic therapy experiments, cells were seeded in 96-well plates (TPP) at density of 10,000 cells per well (3T3) or 7,500 cells per well (HeLa) 24 h prior an addition of the studied compound. The plates were coated with gelatine for experiments with 3T3 cells.

Uptake to the cells

To establish the time profile of intracellular accumulation of compound **5**, HeLa cells were seeded in 6 cm petri dishes at density of 45,000 cells per dish. Cells were left to attach for 24 h and then the medium was removed and 6 μM compound **5** was added in 3 ml of cultivation medium. After 2, 4, 8 or 24 h, the cells were washed three times with 5 ml of phosphate buffered saline (PBS, Sigma) followed by addition of 5 ml of medium. Cells were scraped and transferred to 15 ml centrifugation tubes (TPP) and centrifuged 5 min at 70 × g. Supernatant was replaced with 2 ml of fresh medium, cell pellet was gently resuspended and centrifuged again. This was repeated two times. After the last centrifugation, the medium was replaced with lysis buffer (1% acetic acid in 1:1 Milli-Q water and ethanol). Lysis of cells was performed for 30 minutes and the fluorescence of soluble compound **5** (Figure S20) was measured in black 96-well plates with transparent bottom (Corning, U.S.A.) at λ_{exc} = 364 nm and λ_{em} = 688 nm using Tecan Infinite 200M plate reader (Tecan). Non-specific fluorescence of HeLa cells alone or due to binding of cationic compound to petri dishes was excluded by control experiments (Figure S21). Uptake experiments were performed in duplicate.

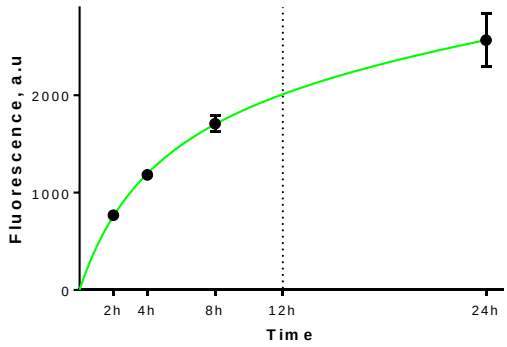

Fig. S20. Uptake of compound **5** by HeLa cells. Points represent mean of two independent experiments, curve is the best non-linear fit.

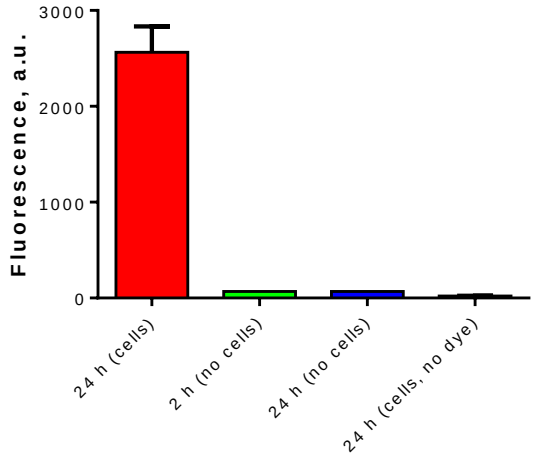

Fig S21. Control experiments for uptake study. In all case the procedure was as described above for uptake. Red – HeLa cells with **5**. Green, blue – petri dishes with **5**, without any cells for 2 h or 24 h, respectively. Black – HeLa cells without presence of complex **5**.

Dark toxicity experiments and photodynamic treatment.

The own toxicities of the compounds without the presence of light (dark toxicity) were assayed at wide concentration range going from 1 to 1000 μM after 24 h incubations. Viabilities of 3T3 or HeLa cells were determined using neutral red (NR) uptake assay (Sigma) based on ability of living cells to incorporate NR in their intact lysosomes. Soluble NR was measured as its optical density at λ = 540 nm using Tecan Infinite 200M plate reader (Tecan, Austria). The viability of experimental groups was expressed as percentage of untreated controls (100%).

For photodynamic treatment experiments, HeLa cells were first loaded for 12 h with various concentrations (0.003 – 10 μM) of compound **5**. After loading, the cells were washed with PBS and fresh medium was added. Irradiation of HeLa cells with light was performed using 450 W ozone-free Xe lamp (Newport) with intensity reduced to 400 W (λ > 570 nm, 12.4 mW/cm^2, 15 min, 11.2 J/cm^2), with long pass filter (Newport OG570) and water filter (8 cm) to eliminate undesirable wavelengths. After irradiation, the cells were incubated another 24 h before assaying their viability by NR as described before. At least five independent experiments, each in quadruplicate, were performed.

Fluorescence microscopy

HeLa cells in cytospin chambers were exposed to 6 μM compound **5** for 12 hours. Prior to visualization of fluorescence, cells were exposed to MitotrackerGreen (Invitrogen-Molecular Probes, Inc., Carlsbad, Ca, USA, 50 nM, 25 minutes, 37°C) and LysotrackerBlue (Invitrogen-Molecular Probes, Inc., Carlsbad, Ca, USA, 25 nM, 25 minutes, 37°C), rinsed with PBS and mounted. The localization and intensity of fluorescence were examined under wide-field fluorescence microscope (Nikon Eclipse E 400 (Nikon Corporation, Kanagawa, Japan)) equipped with the digital color matrix camera COOL 1300 (VDS, Vosskühler, Osnabrück, Germany), using specific filters for red (EX 350-400 and BA 630lp), green (EX 450-490 and

BA 520) and blue (EX 330-380 and BA 420) channels and analyzed by Lucia NIS-Elements AR 3.22 (Fig. S22).

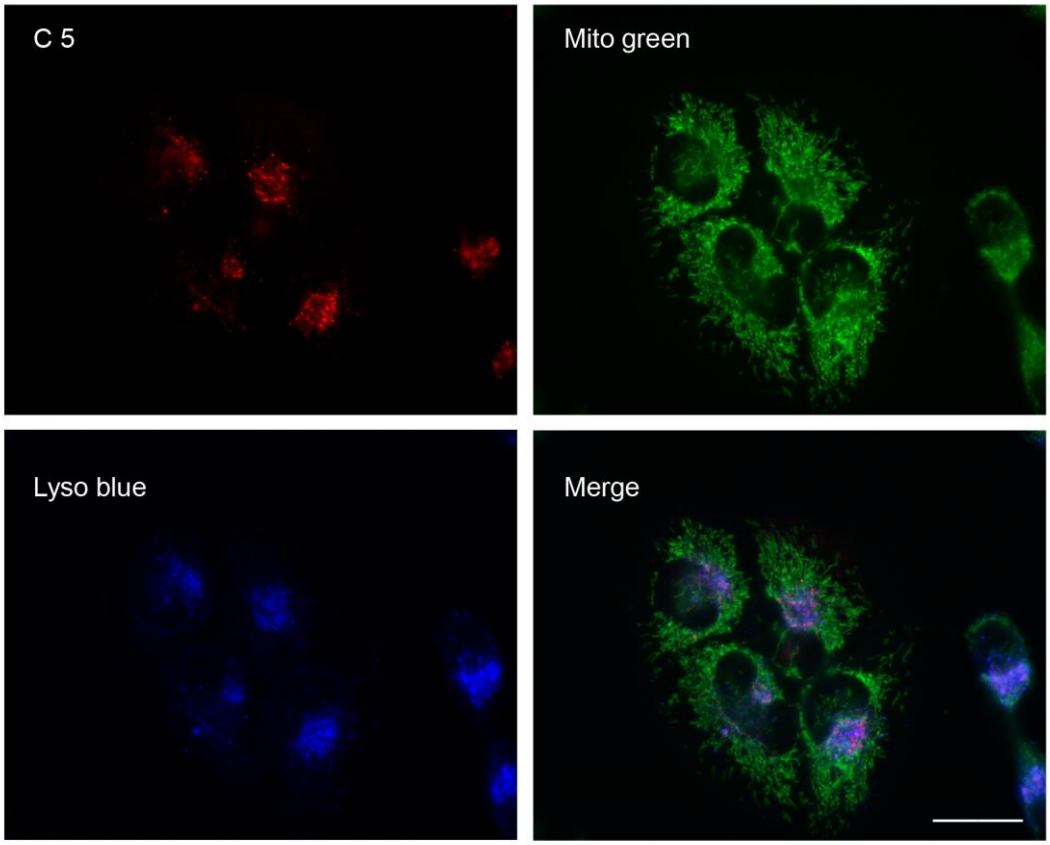

Fig S22. Subcellular localization of compound **5** in HeLa cells. Red channel – fluorescence of compound **5**, green channel – visualization of mitochondria and blue channel – visualization of lysosomes. Fluorescence 600×. Bar 10 μm.

Monitoring of cell death during irradiation – cellular morphology.

An inverted epifluorescence microscope Nikon Eclipse TS100 (Nikon, Japan) equipped with digital cooled camera (1300Q, VDS Vosskühler, Germany) and software NIS-Elements AR 3.10 (Laboratory Imaging, Czech Republic) were used for monitoring of changes in cellular morphology before, during and after irradiation. HeLa cells were seeded on 6 cm petri dishes as described above and incubated 12 h with 1 μM concentration of compound **5**. After washing the petri dish with medium, cells were imaged every 3 minutes – 5×3 min before irradiation, 5×3 min during photodynamic treatment (same conditions as in PDT described above) and after irradiation for another 90 min until no significant changes in cellular morphology was observed. Control experiment involved the same irradiation and monitoring procedure but cells were not incubated with compound **5**. For results see video file (Electronic Supplementary Information).

Table S4. Published data on phototoxicity (IC_{50}) and dark toxicity (TC_{50}) of selected photosensitizers.

Compound	Cells	Incubation	Light dose	IC_{50}	IC_{50}	TC_{50}	TC_{50}	TC_{50} / IC_{50}	Reference
			J/cm^2	μM	μg/mL	μM	μg/mL		
5	HeLa	12 h	11.2 (λ > 570 nm)	0.037	0.18	628	3122	17112	This work
Hematoporphyrin derivative (HpD)	HepG2	4 h	25 (λ = 625 nm)	-	~ 2.5	-	~ 20	8	[9]
Porfimer sodium (Photofrin®)	HepG2	2 h	48 (λ > 610 nm)	-	4.6	-	-	-	[10]
Porfimer sodium (Photofrin®)	HT29	4 h	5 (λ = 640 nm)	-	40[a]	-	> 100	> 2.5	[11]
Pheophorbide A	HT29	4 h	5 (λ = 640 nm)	3[a]	1.8[a]	> 10	> 6	> 3.3	[11]
Temoporfin (Foscan®)	HeLa	18 h	3.5 (λ = 625 nm)	< 0.1[b]	< 0.07[b]	~ 0.8	~ 0.54	> 8	[12]

[a]IC_{90}, [b]complete cell inactivation at concentrations higher than 5 μM.

References

1. D. D. Perrin and W. L. F. Armarego, *Purification of Laboratory Chemicals*, 4th edn., Butterworth Heinemann, Oxford, Boston, 1997.
2. L. Yang, L. Luo, S. Zhang, X. Su, J. Lan, C.-T. Chen and J. You, *Chem. Commun.*, 2010, **46**, 3938-3940.
3. G. M. Sheldrick, *Acta Crystallogr., Sect. A: Found. Crystallogr.*, 2008, **64**, 112-122.
4. P. Zimcik, V. Novakova, K. Kopecky, M. Miletin, R. Z. Uslu Kobak, E. Svandrlikova, L. Váchová and K. Lang, *Inorg. Chem.*, 2012, **51**, 4215-4223.
5. H. J. James and R. F. Broman, *Anal. Chim. Acta*, 1969, **48**, 411-417.
6. M. Montalti, A. Credi, L. Prodi and T. M. Gandolfi, *Handbook of Photochemistry*, 3rd edn., CRC Press, 2006.
7. U. Michelsen, H. Kliesch, G. Schnurpfeil, A. K. Sobbi and D. Wöhrle, *Photochem. Photobiol.*, 1996, **64**, 694-701.
8. R. W. Redmond and J. N. Gamlin, *Photochem. Photobiol.*, 1999, **70**, 391-475.
9. V. Vonarx-Coinsman, M. T. Foultier, L. X. de Brito, L. Morlet, A. Gouyette and T. Patrice, *J. Photochem. Photobiol., B*, 1995, **30**, 201-208.
10. J. T. F. Lau, P.-C. Lo, W.-P. Fong and D. K. P. Ng, *Chem. Eur. J.*, 2011, **17**, 7569-7577.
11. A. Hajri, S. Wack, C. Meyer, M. K. Smith, C. Leberquier, M. Kedinger and M. Aprahamian, *Photochem. Photobiol.*, 2002, **75**, 140-148.
12. M. Garcia-Diaz, D. Sanchez-Garcia, J. Soriano, M. L. Sagrista, M. Mora, A. Villanueva, J. C. Stockert, M. Canete and S. Nonell, *Med. Chem. Commun.*, 2011, **2**, 616-619.